High-resolution study of heavy-ion-induced Kα x-ray spectra of molybdenum atoms

B. Perny, J.-Cl. Dousse, M. Gasser, J. Kern, and Ch. Rhême
Physics Department, University of Fribourg, CH-1700 Fribourg, Switzerland

P. Rymuza and Z. Sujkowski
Institute for Nuclear Studies, 05-400 Swierk, Poland
(Received 24 February 1987)

The $K\alpha$ x-ray spectra of molybdenum bombarded with 6.7-MeV/u ^{4}He and 5.5-MeV/u ^{16}O ions were recorded with an on-line curved-crystal spectrometer in the DuMond geometry. The instrumental resolution was approximately 10.5 eV. $K\alpha_1 L^{n=0,1,2,3}$ and $K\alpha_2 L^{n=0,1}$ principal and satellite lines were observed and resolved for the first time for an atom in the mid-Z region. The relative yields, energies, and linewidths were determined. The yields in the ^{16}O-induced spectrum deviate significantly from the binomial distribution. The width and energy shifts indicate additional multiple M-shell ionization.

I. INTRODUCTION

One of the salient features of heavy-ion-induced K-shell ionization is the high probability of producing multiple L-shell vacancies in the same atom.[1-4] The resulting characteristic $K\alpha$ x-ray spectra exhibit a composite structure of "principal" and "satellite" lines. These latter correspond to various configurations of the "spectator" vacancies in the inner shells. The energy shifts of the $K\alpha$ lines due to each additional L-shell vacancy are larger than the natural linewidths, so that the $K\alpha$ x-ray spectra can in principle be resolved into individual L-shell satellite lines (Fig. 1); however, very-high-resolution instruments are required. Such studies have been made[5-10] for "light" heavy-ion-induced ionization in atoms with $Z < 30$. The instrumental resolution obtained with a Van Hamos crystal spectrometer was about 1.1 eV at 2.2 keV (Refs. 9 and 10) and corresponds approximately to the $K\alpha_1$-$K\alpha_2$ energy difference in this Z region. The spacing of the L satellites is much larger here.

For atoms with $Z > 30$ the situation is reversed: Relativistic effects are no longer negligible, and the energy splitting of $K\alpha_1$ and $K\alpha_2$ lines becomes larger than that between satellites; therefore, these are expected to appear between the principal $K\alpha_1$ and $K\alpha_2$ lines. This is illustrated in Fig. 1.

The bent-crystal spectrometer[11] at the Swiss Institute for Nuclear Research (SIN) variable-energy cyclotron in Villigen, Switzerland enables us to measure x rays in the range of 15 to 100 keV with an energy resolution comparable to the natural linewidth (Fig. 1). This high resolution gives a clear distinction between the $K\alpha_1$ and the $K\alpha_2$ lines and their individual satellites.

This paper presents results for ^{4}He- and ^{16}O-induced x-ray spectra on molybdenum. This is the first of a series of experiments with the purpose of studying the inner-shell ionization process associated with interactions of light heavy ions with atoms in the mid-Z region.

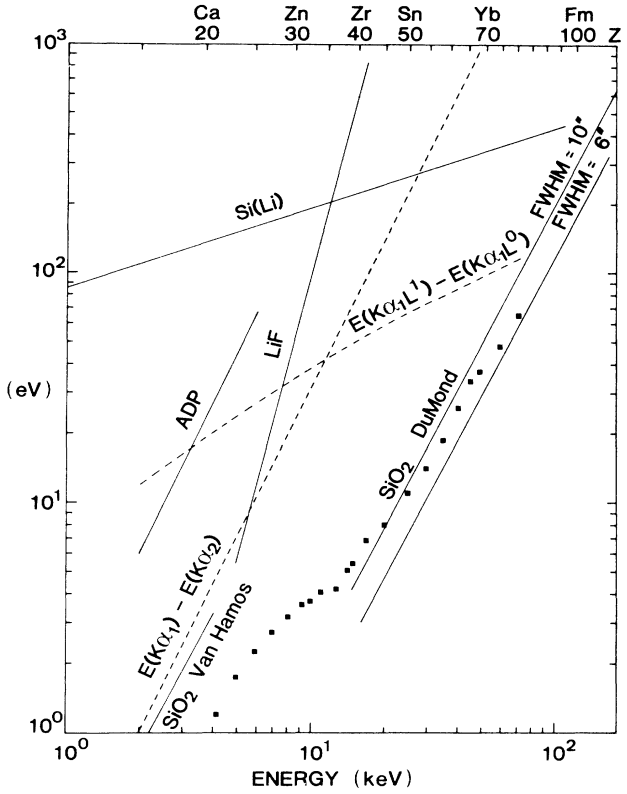

FIG. 1. The energy resolution of a Si(Li) detector compared to that for different types of crystal spectrometers as a function of photon energy. The two lines for the DuMond geometry correspond to the best obtainable and to the best adapted resolution for the present experiments. The figure also shows the energy splitting between $K\alpha_1$ and $K\alpha_2$ lines, $E(K\alpha_1) - E(K\alpha_2)$, as well as that between the $K\alpha$ lines and their satellites $K\alpha L^1$ due to an additional L-shell hole. The natural linewidth of the lines is indicated by the symbol ■. FWHM represents fullwidth at half maximum (in sec of an arc).

II. EXPERIMENT

The crystal spectrometer used for this study is of the DuMond transmission type[12,13] and has a bending radius of 3150 mm. A general description of the facility is presently being prepared[11] and only those elements specific to this experiment will be presented here.

A schematic diagram of the experimental setup is shown in Fig. 2. The spectrometer is positioned at 55° with respect to the incident beam. The (110) reflecting planes of a 1.5-mm-thick quartz crystal plate are used for the diffraction of the x rays. Spectra were collected by step scanning over the desired angular region.

The standard geometry in most experiments with DuMond crystal spectrometers consists of a narrow straight source placed on the focal circle of the bent crystal. To reduce problems arising from the x-ray absorption in the target and from specific in-beam conditions, a DuMond slit geometry is used.[14] The particular requirements for the experiment are as follows:

(i) To achieve an acceptable source strength, the small target width is normally compensated by a larger depth (~ 1 mm) when a conventional DuMond narrow source geometry is used. In this case, as the x-ray absorption in the target is very high, low-energy x rays produced in the rear of the target are absorbed. The modified setup should allow a higher luminosity to be obtained, so that spectra may be measured in a reasonable time. If the energy resolution is to be comparable to the natural x-ray linewidth, the slit width must not, however, exceed ~ 0.1 mm.

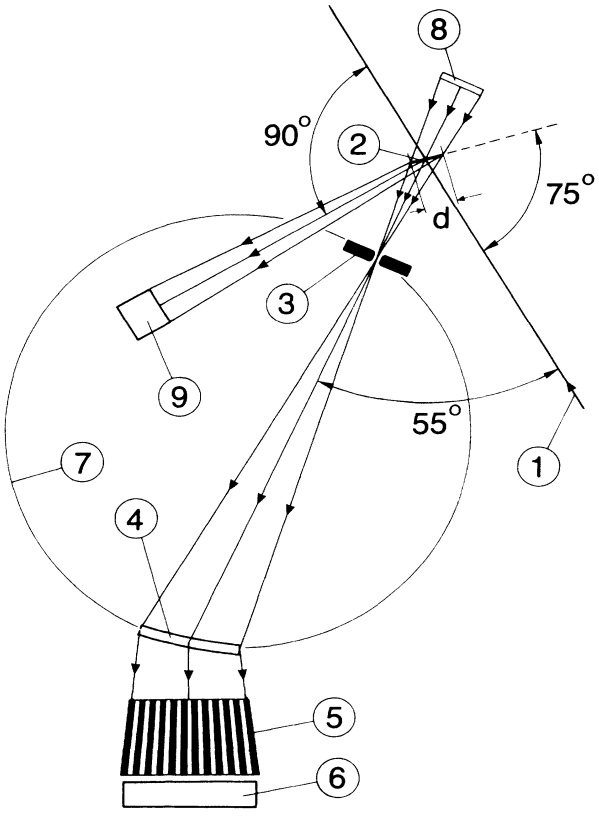

FIG. 2. Schematic diagram of the DuMond slit geometry used in this experiment (not to scale): (1) beam direction, (2) target, (3) tantalum slit, (4) crystal, (5) collimator, (6) detector, (7) focal circle, (8) calibration source (removed during the on-line operation of the instrument), (9) monitor detector.

(ii) In contrast with off-line measurements, the target is exposed to a beam which fluctuates in intensity as well as in position. These must be monitored to allow data normalization.

(iii) The measured line shape depends strongly on the effective source width seen by the crystal. Therefore, thermal target deformations caused by the ion bombardment have to be eliminated.

(iv) A reference line shape must be observed under the same conditions as the in-beam measurements.

In our geometry a slit, 20 mm high and 0.1 mm wide, is placed on the focal circle at a fixed position. The target is placed 40 mm behind the slit and can be larger (Fig. 2) because the slit serves as the effective source of radiation. The target is tilted at 75° to the beam direction and at 130° to the direction target crystal. The beam was focused to a spot having the approximate dimensions 1×15 mm^2. The target depth (d in Fig. 2) corresponds to the beam width. X rays emitted by the whole target surface can be transmitted by the slit for diffraction in the crystal. The absorption of the x rays is determined only by the target thickness and not, as in the conventional DuMond geometry, by the depth d. One disadvantage of the slit geometry is a decrease in solid angle subtended by the target at the crystal. For low photon energies this loss is overcompensated by the lower absorption in the target material. Most importantly, the slit geometry results in a lower sensitive to fluctuations in the beam position and to target deformations due, e.g., to thermal effects.

Normalization of the data at each angular position is provided by subtracting the uncorrelated beam background and dividing the resulting x-ray counts by the integrated x-ray peak measured with a Ge(Li) detector monitor positioned at 90° with respect to the beam line. With this geometry the monitor can account, to a good approximation, for the beam fluctuations in intensity as well as in position.

A ~ 5-Ci ^{161}Tb radioactive source, placed 30 cm behind the slit, was used for the energy calibration[15] and the determination of the instrumental line shape. This arrangement allows the calibration line to be measured under the same conditions as for the in-beam measurements.[14] Some brief comments on other characteristics of the facility are now given.

The peak reflectivity of the crystals was enhanced by a factor of 3 to 4 by applying a high-frequency electric field across it.[15] Periodic deformations of the reflecting planes are introduced by this field and result in an increased mosaicity of the crystal. We used the fifth harmonic of the plate eigenfrequency, i.e., 6543.4 kHz. This technique also allows us to match the intrinsic crystal mosaicity to the chosen slit width so that an optimal reflectivity is obtained.

An optical laser interferometer permits us to determine wavelength ratios with a precision of about 1 ppm in the angular range of the $K\alpha$ x rays. The x rays were recorded

with a thin phoswich (a product of Harshaw Chemical Company, Solon, Ohio) scintillation detector in coincidence with the cyclotron beam burst. The natural background could be reduced by about a factor 2. Figure 3 shows such prompt spectra.

The energy calibration is based on the 48.915 62(14)-keV γ line (Ref. 16) in the decay of ^{161}Tb measured in third order of reflection. This line differs by only 0.5° in angular position from the $K\alpha$ lines in first order of reflection. Nonlinearities of the optical interferometer are negligible for this small angular range. Measurements were performed before and after each run. The instrumental line shape was obtained from the 25.7-keV γ-ray line from the ^{161}Tb source measured in first order of reflection. The same slit-to-crystal distance was used for all measurements. This result in a small increase of the linewidth with respect to exact focusing conditions.

The $^4He^+$ and $^{16}O^{4+}$ ions with, respectively, 28- and 112-MeV initial energy, were delivered from the SIN variable-energy cyclotron. After passing a 5.3-mg/cm^2-thick Havar entrance window in the target chamber, the energies are degraded to 27 and 99 MeV, respectively. The charge state of the ^{4}He and ^{16}O ions are 2^+ and 8^+, respectively, i.e., the particles are totally ionized.

Self-supporting natural metallic foils of natural molybdenum, with thicknesses of 25 mg/cm^2 for the ^{4}He and 12.5 mg/cm^2 for the ^{16}O beam, were used as targets. If we take into account self-absorption, stopping power in the target and energy dependence of K-shell ionization cross sections, we obtain effective energies for the production of the x rays of $\sim$6.7 MeV/nucleon for ^{4}He and $\sim$5.5 MeV/nucleon for the ^{16}O beam. The ^{4}He beam current was 4 μA, and the ^{16}O beam current was 150 nA.

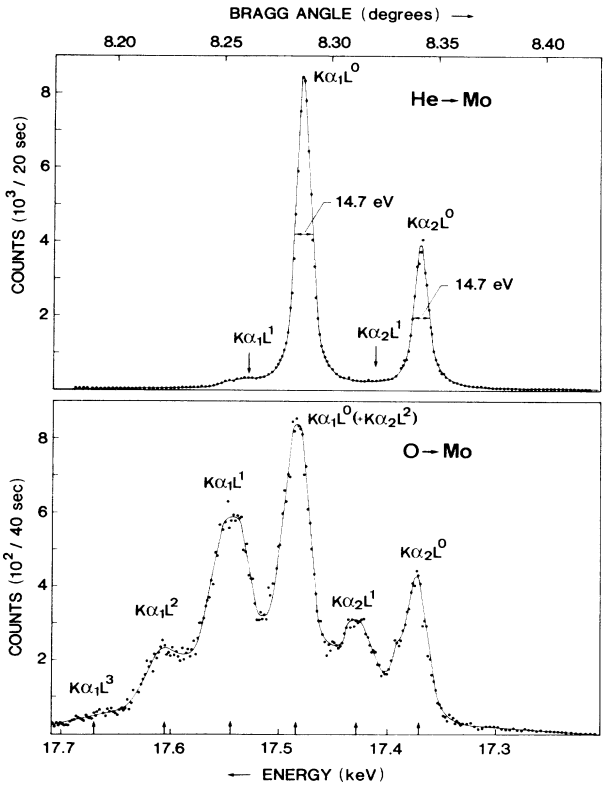

FIG. 3. High-resolution crystal spectrometer spectra of molybdenum $K\alpha$ x rays induced by ^{4}He and ^{16}O ions. The centroid positions are marked with arrows in the oxygen-excited spectrum. In the background regions only every other point is plotted.

III. RESULTS

Figure 3 shows the Mo $K\alpha$ spectra produced with ^{4}He and ^{16}O ions measured on the right side in first order of reflection. The approximate data-taking times were 3.5 hours with ^{4}He and 5 hours with ^{16}O. The background ($\sim$0.25 counts/s) was not affected by the presence of the beam on the targets; therefore, the peak-to-background ratio is determined mainly by the incident beam intensity.

The peaks labeled $K\alpha L^n$ are satellite lines originating from states having one K-shell and n L-shell vacancies in the initial state. To obtain a good energy calibration and to check the reproducibility, the spectrum was measured on both sides of reflection. The spectrometer efficiency for the $K\alpha_1$ and $K\alpha_2$ lines does not differ by more than 1% and no corrections were necessary.

The spectra were analyzed by fitting Voigt functions (convolution of the Gaussian instrumental response with a Lorentzian line shape) to the data using the computer code MINUIT.[17] Experimental peak centroid energies and calculated energy shifts are listed in Tables I and II, relative peak intensities are summarized in Table III and averaged widths in Table IV.

Several interesting features can be noted from the spectra of Fig. 3 and Tables I–IV. (1) Strong satellite peaks with n up to 3 dominate the ^{16}O-induced spectrum. In the ^{4}He-induced spectrum the satellite peaks are observed only as weak shoulders on the high-energy side of the principal lines. (2) The linewidths in the helium-excited spectrum (14.7 eV) are in agreement with the line shape expected from the instrumental resolution, under the effective slit-to-crystal focal conditions, and from the natural x-ray linewidth. The linewidths in the oxygen-induced spectrum are larger than expected if only L-shell vacancies are taken into account. (3) The widths of the satellites in the oxygen-induced spectrum are significantly larger than those of the diagram lines $K\alpha_1L^0$ and $K\alpha_2L^0$ and (4) the diagram lines are shifted towards higher energies in the oxygen-excited spectrum only.

IV. DISCUSSION

A. X-ray energies

The measured energy values and the energy differences with respect to those for singly ionized atoms are compared in Tables I and II with those calculated using the relativistic Dirac-Fock computer code of Desclaux.[18] For all calculations a point-charge nucleus was assumed, and the average-of-configuration $K\alpha$ x-ray satellite transition energies were obtained by taking the difference in the total energies of the single initial and final state. Accordingly, each additional L vacancy increases the x-ray energies by

TABLE I. $K\alpha$ x-ray energies of Mo for ^{4}He bombardment.

x-ray peak	Initial[a] configuration $1s_{1/2}$	$2s_{1/2}$	$2p_{1/2}$	$2p_{3/2}$	E_{expt} (keV)	Energy difference Present work[b] (eV)	Calc.[a] (eV)
$K\alpha_1 L^0$	1	2	2	4	17.4791(5)	0.0±0.5	0
$K\alpha_1 L^1_{I,III}$	1 / 1	1 / 2	2 / 2	4 / 3	17.5270(10)	48±2	49.4 / 50.1 (49.6)
$K\alpha_1 L^1_{II}$	1	2	1	4	17.5450(10)	66±2	(61.5)
$K\alpha_2 L^0$	1	2	2	4	17.3744(5)	0.0±0.5	0
$K\alpha_2 L^1$	1 / 1	1 / 2	2 / 2	4 / 3	17.4230(15)	49±2	47.5 / 51.0 (49.4)

[a]Only the configurations with the lowest and highest x-ray energies are noted. The reported values have been computed by the program for the given configuration directly. Other values can be estimated from Table V. The energy differences in parentheses are statistically weighted averages of the Dirac-Fock differences for the various configurations.
[b]The energy differences are relative to the values quoted by Bearden (Ref. 19).

an amount of the order of 50 eV. Each M vacancy shifts the $K\alpha$ transitions by about $+6$ eV for a $3p$ and -1 eV for a $3d$ electron (more details are given in Table V). Shifts due to N-shell vacancies are too small to be observed in this experiment. The calculated values in Table V are averaged and have been obtained by removing all electrons from a subshell and assuming that the shifts are proportional to the number of holes present. The calculated principal $K\alpha_1$ and $K\alpha_2$ transition energies (17.482 and 17.377 keV) are 3 eV higher than the experimental

TABLE II. $K\alpha$ x-ray energies of Mo for ^{16}O bombardment.

x-ray peak	Initial[a] configuration $1s_{1/2}$	$2s_{1/2}$	$2p_{1/2}$	$2p_{3/2}$	E_{expt} (keV)	Energy difference Present work[b] (eV)	Calc.[a] (eV)
$K\alpha_1 L^0$	1	2	2	4	17.485(1)	6±1	0
$K\alpha_1 L^1$	1 / 1	1 / 2	2 / 1	4 / 4	17.542(2)	63±2	49.4 / 61.4 (52.5)
$K\alpha_1 L^2$	1 / 1	0 / 2	2 / 0	4 / 4	17.604(2)	125±2	99.0 / 123.6 (106.0)
$K\alpha_1 L^3$	1 / 1	0 / 2	2 / 0	3 / 3	17.661(5)	182±6	150.3 / 175.9 (160.3)
$K\alpha_2 L^0$	1	2	2	4	17.379(1)	5±1	0
$K\alpha_2 L^1$	1 / 1	1 / 2	2 / 2	4 / 3	17.428(2)	54±2	47.4 / 50.8 (49.4)
$K\alpha_2 L^2$	1 / 1	0 / 2	2 / 2	4 / 2			95.5 / 102.7 (99.8)

[a]See footnote a Table I.
[b]See footnote b of Table I.

TABLE III. Relative $K\alpha$ x-ray satellite intensities for Mo bombarded by 6.7-MeV/amu ^{4}He and 5.5-MeV/amu ^{16}O projectiles.

x-ray peak	^{4}He	^{16}O
$K\alpha_1L^0$	100±1	100±1
$K\alpha_1L^1_{I,III}$	2.5±0.5	102±10
$K\alpha_1L^1_{II}$	2.0±0.4	
$K\alpha_1L^2$		29±3
$K\alpha_1L^3$		0.8±0.3
$K\alpha_2L^0$	48.0±0.5	40±4
$K\alpha_2L^1$	1.7±0.3	40±4
$K\alpha_2L^3$		(11±2)[a]

[a]Derived assuming the same ratios as for the $K\alpha_1$ lines.

energies of Bearden.[19] Since the predictions of the energy shifts should be much more accurate than those of the absolute energy values, we normalized the calculated $K\alpha_1$ and $K\alpha_2$ transition energies to the values given in Ref. 19.

^{4}He-induced spectrum: Analysis of the data showed that both the $K\alpha_1L^0$ and $K\alpha_2L^0$ lines are symmetric. Their energies are in excellent agreement with the values quoted by Bearden.[19] The Doppler effect does not contribute any sizable broadening and energy shift (see the Appendix).

The $K\alpha_1L^1$ shape cannot be reproduced with a single peak having a shape similar to the $K\alpha_1L^0$ one. Theoretical calculations predict shifts of 50 and 61 eV, respectively, for the $K\alpha_1$ line when an additional $2p_{3/2}$ or $2s_{1/2}$ hole, or a $2p_{1/2}$ hole, is present (Table V). The results of a fit of the $K\alpha_1L^1$ peak with two lines, shown in Table I, agrees very well with this prediction. Consequently, a possible interpretation is that the $K\alpha_1L^1$ peak is a composite of two satellite lines due to a missing electron in the $(2s_{1/2},2p_{3/2})$ and $(2p_{1/2})$ shell, respectively. One difficulty with this interpretation is that the expected intensity ratio is 5:2 (roughly the ratio of the number of L-shell electrons available) and the experimental value is 2.5(5):2.0(4).

For the $K\alpha_2L^1$ transition, the shifts due to a $2p_{3/2}$ and $2p_{1/2}$ hole are expected to be 51 and 49 eV, respectively, so that only one peak can be observed experimentally. In fact, the $K\alpha_2L^1$ peak seems to consist of a single peak in agreement with this prediction (Table V).

^{16}O-induced spectrum: In contrast to the ^{4}He-induced spectrum, the line shapes of the ^{16}O-induced x rays cannot be reproduced with one Voigt function. Due to multiple M-shell vacancies, the lines are much broader and slightly asymmetric (see Sec. IV C). Similar effects have been observed in Ti by Hill *et al.*[8]

To extract the centroids, several Voigt profiles were fitted at the peaks until the overall shape of the spectrum was reproduced. The centroid positions are listed in Table II and indicated on Fig. 3 by arrows.

The principal $K\alpha_1$ and $K\alpha_2$ lines are shifted by about 5 to 6 eV towards higher energies relative to those in the helium-induced spectrum. The asymmetry of the $K\alpha_2L^0$ peak is observed on both sides of reflection and is statistically significant. The $K\alpha_1L^0$ peaks seems to be symmetric but in this case the underlying $K\alpha_2L^2$ satellite might have smeared the asymmetry beyond recognition. Asymmetric broadening and net energy shifts are the expected results of multiple M-shell ionization.

It should be stressed, however, that in contrast with the L-shell ionization, it is not possible to deduce the degree of M-shell ionization from the energy shifts in a model-independent way, since different M subshells contribute both positive and negative shifts (Table V).

In molybdenum only L_1-L_3X Coster-Kronig transitions can occur.[20,21] Because $2s_{1/2}$ and $2p_{3/2}$ holes give nearly the same energy shifts, our spectra should be influenced by these transitions.

As for ^{4}He-induced spectra, the Doppler effect produces only negligible shift and broadening contributions (see Appendix).

TABLE IV. Average widths in eV of Mo $K\alpha$ satellites (the expected linewidth is 14.7 eV).

x-ray peak	^{4}He (eV)	^{16}O (eV)
$K\alpha_1L^0$	14.7±0.5	30±1
$K\alpha_1L^1$	a	38±2
$K\alpha_1L^2$		41±2
$K\alpha_1L^3$		
$K\alpha_2L^0$	14.7±0.5	20±2[b]
$K\alpha_2L^1$	a	40±2

[a]The peaks $K\alpha_1L^1_{I,III}$, $K\alpha_1L^1_{II}$, and $K\alpha_2L^1$, respectively, have been fitted with the same shape as the $K\alpha_1L^0$ one.
[b]The shoulder on the left side is not included.

TABLE V. Calculated $K\alpha_1$ and $K\alpha_2$ average energy shifts due to one additional L-, M- or N-shell vacancy (Ref. 19) (see Sec. IV A).

Vacancy	$\Delta E(K\alpha_1)$ (eV)	$\Delta E(K\alpha_2)$ (eV)
$2s_{1/2}$	49.4	47.5
$2p_{3/2}$	50.1	51.0
$2p_{1/2}$	61.5	49.0
$3s_{1/2}$	4.7	4.6
$3p_{3/2}$	6.5	5.0
$3p_{1/2}$	6.2	8.7
$3d_{5/2}$	−0.5	−1.9
$3d_{3/2}$	−1.6	0.6
$4s_{1/2}$	0.6	0.0
$4p_{3/2}$	0.6	0.6
$4p_{1/2}$	0.7	1.1
$4d_{5/2}$	−0.16	−0.3
$4d_{3/2}$	0.25	−0.1

B. X-ray intensities

The observed satellite yield ratios in the oxygen-induced $K\alpha$ x-ray spectrum, $I(KL^0):I(KL^1):I(KL^2):I(KL^3)=100:102:29:0.8$ (Table III), correspond to the initial L-shell vacancy distribution modified by the radia-

tive, Auger, and Coster-Kronig transitions. Assuming the corresponding transition rates to be the same as for atoms ionized only in the K and L shells,[20,22] we obtain, using the statistical procedure of Ref. 23, an initial L-vacancy distribution 100:173:57:1.7.

To study the effect of additional M-shell vacancies we assume the ionization probability per M-shell electron to be $P_M = 0.16$, which is compatible with the observed net energy shifts of the $K\alpha_1 L^0$ line if we take the calculated shifts for various M-subshell electrons (Table V). The resulting vacancy distribution is 100:152:48:1.4. It is seen that the effects of the M-shell ionization on the yield ratios are noticeable but not very pronounced. None of these deduced ionization yield distributions is compatible with a binomial distribution. Assuming for the latter a $I(KL^0):I(KL^1)$ yield ratio equal to the value deduced from the experiment, i.e., 100:152, we obtain the relative yields 100:152:102:39.

The observed strong deviations from the binomial distribution can be taken as evidence for contributions to the L-shell ionization from effects other than direct uncorrelated ionization by impact. One such effect which may be expected to contribute strongly in the present case is L-shell electron capture by the projectile.

C. Widths of diagram and satellite lines

An interesting property of the ^{4}He- and ^{16}O-induced spectra is the linewidth of the diagram and satellite peaks (Table IV). The expected linewidth contributions come from the natural atomic linewidth, instrumental resolution, unresolved shifts due to outer-shell multiple ionization, and target-recoil Doppler broadening.

For our experimental conditions, Doppler broadening is expected to contribute about 1.32 eV for the ^{16}O beam and is negligible for ^{4}He (see the Appendix). From energy-level calculations,[18] shifts caused by the loss of N-shell electrons are about ten times smaller than those due to M-shell electrons (Table V) and are therefore not expected to have a significant influence on our results.

The experimental $K\alpha_1 L^0$ and $K\alpha_2 L^0$ linewidths (14.7 eV) in the helium-excited spectrum are in agreement with the linewidth expected from the instrumental resolution (10.5 eV) and the natural x-ray linewidth (6.8 eV). The instrumental resolution is not the best possible since, for technical reasons, the γ-ray and x-ray spectra were observed using a constant slit-to-crystal distance.

In the oxygen-induced spectrum the principal and satellite lines are much broader (see Table IV). The larger widths can very probably be ascribed to unresolved KL^nM^m satellites and multiplet lines arising from states of various angular momentum couplings of the electrons or the vacancies.

V. SUMMARY AND CONCLUSIONS

Multiple inner-shell ionization phenomena in medium-heavy atoms have been studied for the first time using a high-resolution bent-crystal spectrometer. The $K\alpha$ x-ray spectrum of Mo bombarded with ^{16}O ions reveals a rich structure of resolved L-shell satellites. The intensity ratios of these satellite lines deviate significantly from those of a binomial distribution. This indicates the presence of effects other than direct uncorrelated ionization by impact, such as electron capture by the projectile.

The energies and the linewidths found in the ^{16}O spectrum indicate strong effects from simultaneous multiple M-shell ionization. In contrast to the L-shell satellites, the degree of M-shell ionization cannot be deduced from the energy shifts alone, because the various M subshells contribute to the shifts with opposite signs. Qualitatively, this is borne out by a simple relativistic Dirac-Fock calculation. Quantitative analysis of the energy shifts and of the line profiles requires a dynamical collision model taking into account the various angular momentum couplings among the electrons involved.

Further experiments are in progress, including systematic studies of the $K\alpha$ x-ray spectra as a function of Z in the mid-Z region and a detailed analysis of the $K\beta$ spectra.

ACKNOWLEDGMENTS

This work was supported in part by the Swiss Institute for Nuclear Research (SIN) and by the Swiss National Science Foundation. The authors are very grateful to Dr. S. Jaccard and Dr. Th. Stammbach and the cyclotron crew for excellent beam conditions. They thank S. Drack for the development of an intense oxygen-ion source and Dr. F. Atchison for his valuable comments.

APPENDIX

Doppler effect

The Coulomb deflection angle θ of an incident projectile of kinetic energy T and charge $Z_1 e$ impinging on a target atom of charge $Z_2 e$ at a distance p (impact parameter) is given by

$$\theta = 2 \arctan\left[\frac{R}{2p}\right], \tag{1}$$

where R is the collision diameter:

$$R = \frac{Z_1 Z_2 e^2}{4\pi\epsilon_0 T} . \tag{1a}$$

From θ, T, and the masses M_1 (projectile) and M_2 (target atom), the recoil energy E_R, and angle α_R of the atom can be calculated. Since the mean lifetime of an electron hole is very short ($\sim 10^{-16}$ sec) compared to the recoil time of the atom ($\sim 10^{-12}$ sec), it is quite a good approximation to assume that the x ray is emitted by the atom at the maximum velocity v_R:

$$v_R = \left[\frac{2E_R}{M_2 c^2}\right]^{1/2} c , \tag{2}$$

where c is the velocity of light in a vacuum.

If γ is the angle between the recoil direction and the target-crystal direction, the observed energy of the x rays emitted by the moving atom will be

$$E \cong (1 + \beta_R \cos\gamma) E_0 , \tag{3}$$

where $\beta = v_R/c$ and E_0 is the x-ray energy of the atom at rest. For a given impact parameter p, the atom moves somewhere along the surface of a cone of aperture $2\alpha_R$ so that $\cos\gamma$ can be expressed as a function of the azimuthal angle ε (see Fig. 4):

$$\cos\gamma = \sin\alpha_R \sin\Omega \sin\varepsilon - \cos\alpha_R \cos\Omega \ . \tag{4}$$

The averaged x-ray energy observed by the crystal spectrometer for a given impact parameter p is then

$$E_p = E_0 \left[1 + \frac{\beta_R}{2\pi} \int_0^{2\pi} \cos\gamma \, d\varepsilon \right] = E_0 (1 - \beta_R \cos\alpha_R \cos\Omega) \ . \tag{5}$$

Doppler shift

The energy shift of the observed x-ray line is obtained by taking the sum over p of $(E_p - E_0)$, weighted by the factor $I_p p$, I_p being the ionization probability for the considered projectile and target atom at the impact parameter p:

$$\Delta E = \frac{-E_0 \cos\Omega \int_0^{\infty} \beta_R \cos\alpha_R I_p \, p \, dp}{\int_0^{\infty} I_p p \, dp} \ . \tag{6}$$

If the thickness of the target is not negligible, the energy loss of the projectiles and the self-absorption of the x rays in the target must be taken into account, leading to

$$\Delta E = \frac{-E_0 \cos\Omega \int_0^{h} \int_0^{\infty} \beta_R \cos\alpha_R I_p p \sigma_K(x) e^{-\mu\rho(x/\cos\phi)} dp \, dx}{\int_0^{h} \int_0^{\infty} I_p \sigma_K(x) p \, dp \, dx} \ . \tag{7}$$

In the above relation, h is the thickness of the target, $\mu\rho$ its attenuation factor for the considered x rays, ϕ the angle between the direction of observation and the normal to the target, and $\sigma_K(x)$ is the cross section for K-shell ionization at the depth x inside the target. It should be noticed that the crystal solid angle does not appear in relation (7), since it contributes only to the broadening of the line and not to the shift.

Doppler broadening

In order to obtain the Doppler broadening, the original Lorentzian distribution $L(u)$ of the x rays has to be folded with the function $D(u)$ describing the distribution of the Doppler-shifted x rays (where u is the energy difference $E - E_0$). To determine $D(u)$, a Monte Carlo computer code has been written. Each event is characterized by five parameters which are selected randomly: depth x in the target where the ionization takes place, impact parameter p, azimuthal angle ε and coordinates x_c and y_c of the point where the x ray impinges on the diffraction crystal surface. For each incident projectile, the code first picks the five parameters, then computes the energy difference u, and finally scores an event in the energy channel corresponding to u.

The depth x is randomly picked between 0 and h, with the condition to follow the distribution function $g(x)$ given by

$$g(x) = \sigma_K(x) e^{-\mu\rho(x/\cos\phi)} \tag{8}$$

where $\sigma_K(x)$ is the cross section for K-shell ionization for a projectile of energy $E_1(x/\cos\psi)$, ψ being the angle between the incident beam and the normal to the target. The x values are generated by solving the following integral equation:

$$\int_0^{x} \sigma_K(s) e^{-\mu\rho(s/\cos\phi)} ds = z_x \int_0^{h} \sigma_K(s) e^{-\mu\rho(s/\cos\phi)} ds \ , \tag{9}$$

where z_x is a random number uniformly distributed in the open interval 0 and 1.

Similarly, the randomized impact parameter p_r is obtained from the integral equation

$$\int_0^{p_r} I_p p \, dp = z_p \int_0^{\infty} I_p p \, dp \ , \tag{10}$$

where z_p is another random number uniformly distributed between 0 and 1. The distribution of the angles ε and coordinates x_c and y_c being uniform, these are directly generated from three uniformly distributed random numbers.

The cross sections $\sigma_K(x)$ are determined by a plane-wave Born approximation (PWBA) calculation,[24] which includes corrections for increased binding energy and polarization effect,[25] and also taking into account corrections for Coulomb deflection[26] and relativistic effects of the K-shell electron wave function.[27]

The ionization probabilities I_p are taken from the tables of Hansteen *et al.*[28] The code also computes the average value of u, giving a direct estimate of the Doppler shift. The shifts calculated in this way are statistically consistent with the results given by the analytic expression (7).

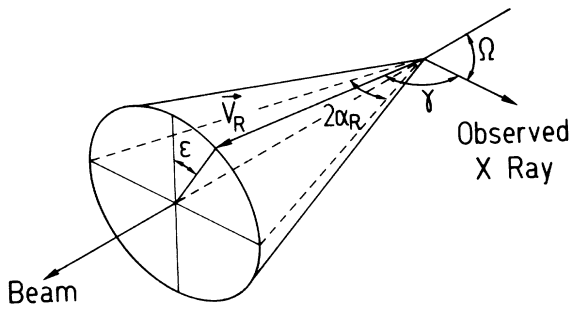

FIG. 4. Schematic geometrical diagram for the evaluation of the Doppler effect.

Results

For the 12.5-mg/cm^2-thick Mo target bombarded by 99-MeV ^{16}O projectiles, the broadening of the $K\alpha_1$ line

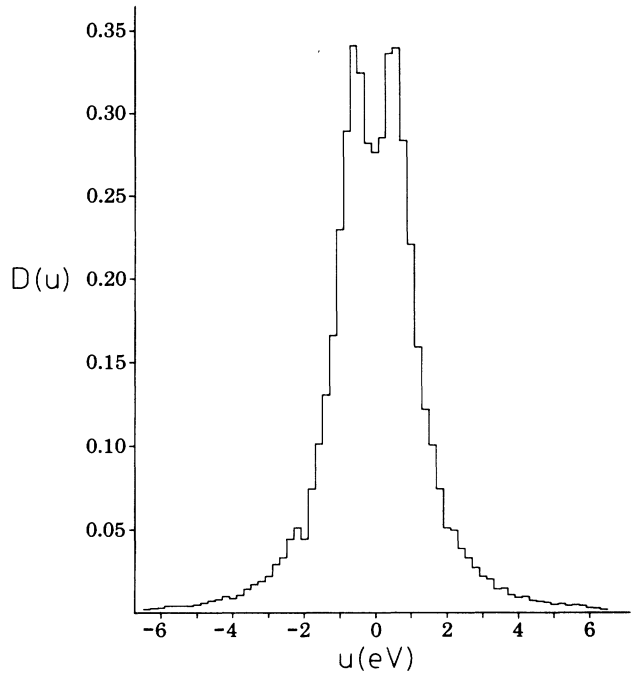

FIG. 5. Energy difference distribution $D(u)$ arising from the Doppler effect. The computation has been performed for 17.48-keV monoenergetic x rays emitted by a 12.5-mg/cm^2-thick molybdenum target bombarded by 99-MeV ^{16}O projectiles. The Monte Carlo simulation calculated 50 000 events. The tails of the distribution extend much farther than represented here (events with energy differences up to $u \sim 100$ eV have been obtained; see, however, comment in the text).

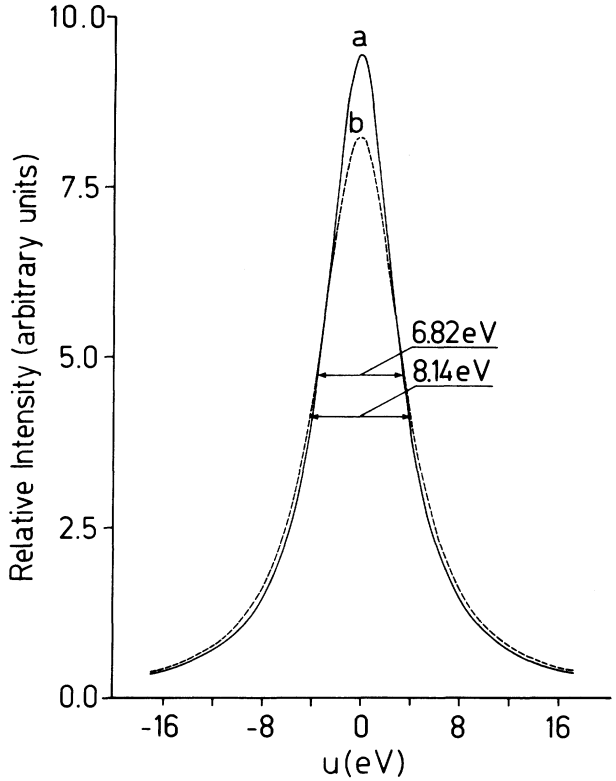

FIG. 6. Shape of the $K\alpha_1$ x-ray of molybdenum. (a) without Doppler effect, (b) with Doppler effect (dashed curve, calculated with the same conditions as stated in Fig. 5).

(natural linewidth 6.82 eV) is 1.32 eV while the shift of the line is smaller than 0.05 eV. The distribution $D(u)$ corresponding to this case is illustrated in Fig. 5; the shape of the broadened line is compared to that of the pure Lorentzian one in Fig. 6. The latter shows also that the tails of the broadened line have a slightly increased intensity. This, however, does not affect significantly the measured spectrum, the relative increase of the apparent background due to the enhanced tails being only a few percent.

For the 25-mg/cm^2-thick Mo target bombarded by 28-MeV ^{4}He projectiles, the broadening of the line is only 0.13 eV, the shift being negligibly small ($< 10^{-3}$ eV). This calculation gives an upper limit for the Doppler shift and broadening, since the probability of events at small impact parameters (and thus with the largest energy differences) is strongly reduced by the competing nuclear reactions.

Doppler shifts and broadenings of the $K\alpha$ satellite lines are expected to be of the same order of magnitude as those calculated for the $K\alpha_1$ principal line because the mean values of the impact parameter for a K-shell single ionization and for a K-shell + L-subshell double ionization are approximately equal [$\bar{p}(K) = 1.36 \times 10^{-2}$ Å, $\bar{p}(K + L_1) = 1.29 \times 10^{-2}$ Å, $\bar{p}(K + L_2) = \bar{p}(K + L_3) = 1.31 \times 10^{-2}$ Å].

[1]*Methods of Experimental Physics*, edited by P. Richard (Academic, New York 1980), Vol. 17, and references therein.

[2]B. Crasemann, *Atomic Inner-Shell Physics* (Plenum, New York, 1985) and references therein.

[3]Proceedings of the Third International Conference on Proton-Induced X-ray Emission and its Analytical Applications, Heidelberg, 1983, edited by B. Martin [Nucl. Instrum. Methods B **3**, 231 (1984)].

[4]Proceedings of the Eighth International Conference on Application of Accelerators in Research and Industry, Denton, 1984, edited by J. L. Duggan, I. L. Morgan, and J. A. Martin [Nucl. Instrum. Methods B **10/11**, (1985)].

[5]D. Burch, P. Richard, and R. L. Blake, Phys. Rev. Lett. **26**, 1355 (1971).

[6]A. R. Knudsen, D. J. Nagel, P. G. Burkhalter, and K. L. Dunning, Phys. Rev. Lett. **26**, 1149 (1971).

[7]D. G. McCrary and P. Richard, Phys. Rev. A **5**, 1249 (1978).

[8]K. W. Hill *et al.*, Phys. Rev. A **13**, 1334 (1976).

[9]S. Raman *et al.*, Nucl. Instrum. Methods B **3**, 100 (1984).

[10]C. R. Vane *et al.*, Nucl. Instrum. Methods B **10/11**, 190

(1985).
[11]B. Perny *et al.*, Nucl. Instrum. Methods (to be published).
[12]J. W. M. DuMond, Rev. Sci. Instrum. **18**, 626 (1947) (DuMond's original paper).
[13]J. W. Knowles, Nucl. Instrum. Methods **162**, 677 (1979) (a detailed general description of modern curved crystal spectrometer techniques).
[14]W. W. Sapp. Jr., Nucl. Instrum. Methods **141**, 391 (1977).
[15]J.-Cl. Dousse and J. Kern, Acta Cryst. A **36**, 966 (1980).
[16]B. Jeckelmann *et al.*, Nucl. Instrum. Methods A **241**, 191 (1985).
[17]F. James and M. Roos, Comput. Phys. Commun. **10**, 343 (1975).
[18]J. P. Desclaux, Comput. Phys. Commun. **2**, 31 (1975).
[19]J. A. Bearden, Rev. Mod. Phys. **39**, 78 (1967).
[20]E. J. McGuire, Phys. Rev. A **3**, 587 (1971).
[21]E. J. McGuire, Phys. Rev. A **3**, 1801 (1971).
[22]E. J. McGuire, Phys. Rev. A **2**, 273 (1970).
[23]F. P. Larkins, J. Phys. B **4**, 229 (1971).
[24]R. Rice, G. Basbas, and F. D. McDaniel, At. Data Nucl. Data Tables **20**, 503 (1977).
[25]G. Basbas, W. W. Brandt, and R. Laubert, Phys. Rev. A **17**, 1655 (1978).
[26]R. Anholt, Phys. Rev. A **17**, 983 (1978).
[27]R. Anholt, Phys. Rev. A **17**, 976 (1978).
[28]J. M. Hansteen *et al.*, At. Data Nucl. Data Tables **15/4**, 306 (1975).